Reduced Phototransduction Models for Photoceptors in the Retina of *Drosophila*

Qiuyang Wang[1], **Yiyin Zhou**[2], **Aurel Lazar**[3]

[1] Department of Applied Physics and Applied Mathematics, Columbia University, New York, 10027, U.S.
[2,3] Department of Electrical Engineering, Columbia University, New York, 10027, U.S.

2022/12/23

Abstract

The retina is an interface between the visual world and the visual system of *Drosophila*, whose phototransduction process transforms the optical signals into electrical signals. However, simulating the retina of *Drosophila* is costly due to the complicated physiological basis of phototransduction. Here, we develop a series of Reduced Phototransduction Models (RPMs) based on the dynamics of microvilli in the photoreceptors. The RPMs preserve the behavior of the photoreceptor given a certain optical input with a much faster computational speed. The RPMs also provide a systematic insight into the integrate-and-fire(IF) pattern of the photoreceptors in *Drosophila*.

Keywords: *phototransduction; input-output (I/O) equivalence; integrate-and-fire device; Fokker-Planck equation; cellular signalling network*

1. Introduction

The *Droshophila* visually senses the outer world by their compound eyes. The retina is the first layer of the compound eye, consisting of 700-800 small facets called ommatidia. There are eight photoreceptors in each ommatidium, which is where phototransduction takes place. Such a process transforms the optical signals into the electrical signals, which are further transferred to the deeper layers in the brain, such as the lamina and medulla [1].

A challenge for retina simulation is the complicated algorithm of a single photoreceptor. There are roughly 30,000 Microvilli in each photoreceptor, while each Microvilli is independently defined by a set of seven Ordinary Differential Equations (ODEs). Thus there are in total 210,000 ODEs for a single photoreceptor, which is computationally costly due to the high dimension.

To reduce the dimensionality of the phototransduction process, we systematically studied their integrate-and-fire pattern, based on which we developed a series of Reduced Phototransduction Models (RPMs). The RPMs are an I/O equivalence of the photoreceptors, preserving their behavior given a certain optical input with much less computational cost.

In this paper, we first introduce the parallel processing model of the *Drosophia* retina on GPUs based on the Neurokernel [2]. Next, in section 3, we provide a detailed view of the physiological basis of phototransduction. In section 4, we describe the RPMs with their ODEs definition. We then provide a Partial Differential Equation (PDE) method to capture the dynamic of photoreceptor as a potential RPM in section 5. Finally, in section 6, we briefly review the current RPMs as well as their drawbacks, then discuss the future direction of RPMs and their implementation.

2. A Parallel Processing Model of the *Drosophia* retina

The most fundamental unit of the *Drosophia* retina is photoreceptor. Each photoreceptor in the *Drosophia* is independent of each other, thus performs a complex set of computations on its own, which suggests that the retina works as a parallel visual information pre-processor.

Here, we simplify the visual information of the outer world as a video input. The model is evolved frame by frame. For each frame, we project the squared video frame into a hemisphere, called screen. The retina is a smaller hemisphere lying inside the screen, with photoreceptors uniformly arranged on the retina surface. We assume each photoreceptor is orthogonal to the retina surface associated with an optical axis. A photoreceptor can only receive the input within the optical axis, which results into a receptive field on the screen, as shown in **Figure 1**. The input to the photoreceptor is the Gaussian average of its receptive field.

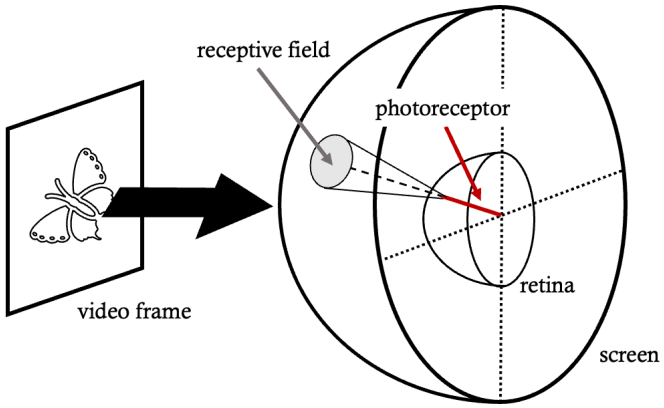

Figure 1. the input of a single photoreceptor given a video frame.

Eight photoreceptors R1-8 forms an ommatidium, where R7/8 are in the center while R1-R6 are wreathed around R7/R8 [3]. The ommatidia are arranged in hexagon arrays in the retina [4].

Such construction allows us to transform the visual input into a parallel photoreceptors pre-processor, where each photoreceptor evolves according to its phototransduction process.

3. The Physiological Basis of Phototransduction

3.1. molecular signalling cascade in phototransduction

Each photoreceptor contains roughly 30,000 microvilli, while every microvillus is independent to each other. Since microvillus is the minimum physiological unit responding to the luminance signal, the phototransduction process can be divided into 30,000 parallel sub-processes. Given an optical input, each microvillus will open a certain number of TRP channels (denoted as X_6) by a stochastic molecular signal cascade. The summation of the openned TRP channels will contribute to the inward current, which will be passed to a non-firing-membrane model and transformed into the output voltage [4] (**Figure 2**).

The single microvillus dynamic is a G protein-mediated signaling pathway transducing single photons into a transient response called quantum bumps with opening of 10-20 TRP channels lasting 20 ms [5]. The major biochemical steps of the signaling cascade are illustrated in **Figure 3**(a). A single photon will be absorbed by rhodopson (R) leading to its activated state (metarhodopsin, M^*), which will activate the G-protein, further activating the PLC molecule. Due to the lack of exact molecular mechanism of TRP channel (here is called B^*), we refer the activator of the TRP channel as a molecular variable A^*, positively regulated by the PLC^* and negatively regulated by a Calcium dependent protein C^*. The opening of TRP channels will cause the influx of Ca^{2+}, activating the C^*, which provides a negative feedback to the upstream molecules M^*, PLC^*, A^* and TRP channels [6].

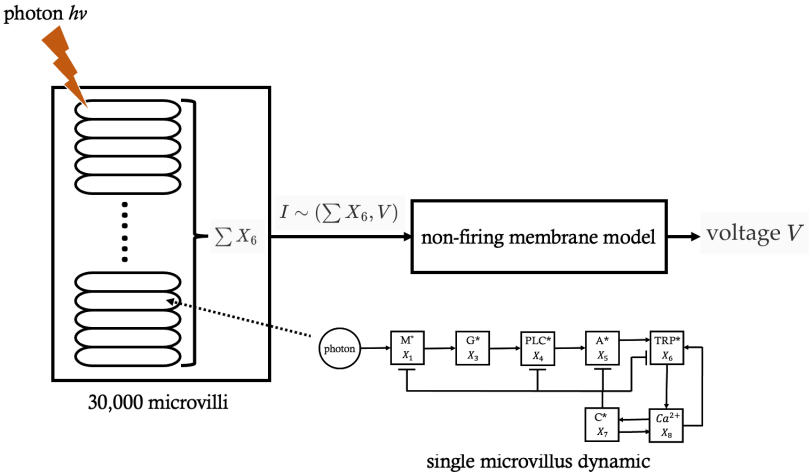

Figure 2. The phototransduction process in a single photoreceptor

Following such physiological observations, Lazar *et al.* developed a quantitive model successfully characterizing the I/O relationship of photoreceptors [4] with the diagram shown in **Figure 3**(b). We refer this model as the Full Model, which will be used as the baseline for RPMs.

The Full Model can be written as a seven variables stochastic ODEs system as following:

$$dX_1 = -\gamma_{X_1}(X_7)X_1dt + dN_t$$
$$dX_2 = (-\kappa_{X_3}X_1X_2 + {}_{X_2}\ (T_4 - X_2 - X_3 - X_4))dt + \sigma_2 dZ_2$$
$$dX_3 = (-\kappa_{X_4}(T_3 - X_4)X_3 + \kappa_{X_3}X_1X_2 - {}_{X_3}\ X_3X_4)dt + \sigma_3 dZ_3$$
$$dX_4 = (\kappa_{X_4}(T_3 - X_4)X_3 - \gamma_{X_4}(X_7)X_4)dt + \sigma_4 dZ_4$$
$$dX_5 = (\kappa_{X_5}X_4 - \gamma_{X_5}(X_7)X_5 - \kappa_{X_6}X_5^2(T_1 - X_6))dt + \sigma_5 dZ_5$$
$$dX_6 = (\kappa_{X_6}(X_8)\frac{X_5^2}{2}(T_1 - X_6) - \gamma_{X_6}(X_7)X_6)dt + \sigma_6 dZ_6$$
$$dX_7 = (\kappa_{X_7}(T_2 - X_7)X_8 - \gamma_{X_7}X_7)dt + \sigma_7 dZ_7$$

where N_t is an Poisson process with intensity λ. Z_i are independent Brownian motion processes.

3.2. transition between different states of microvilli

For a single microvillus, the input is photons and the output is the number of opened TRP channels (X_6). A key observation is that the microvilli will go into a refractory period after a quantum bump. This is because the open of 10-20 TRP channels (quantum bump) will activate the downstream Calcium dependent protein C^*, which gives a negative feedback to upstream molecules (**Figure 4**).

Thus, a single microvillus can have three different states: firing period (x_1), refractory period (x_2) and resting period (x_3). The microvillus will transit through these states with single direction: With the photons activation, the microvillus in the resting period will be activated, thus go into the firing period. After the quantum bump, it goes into the refractory period, which will then be transited into the resting period again after a certain time τ. Hence the microvillus goes back to its initial state again after completing the transition triangle (**Figure 5**).

4. Construction and Performance of RPMs

Due to the large number of microvilli, the Full Model is computationally expensive. Hence, it is necessary to develop RPMs as an I/O equivalence of the Full Model but with less differential equations. Here we develop a series of RPMs following the transition diagram of the microvilli states, and further test their performance compared to the Full Model.

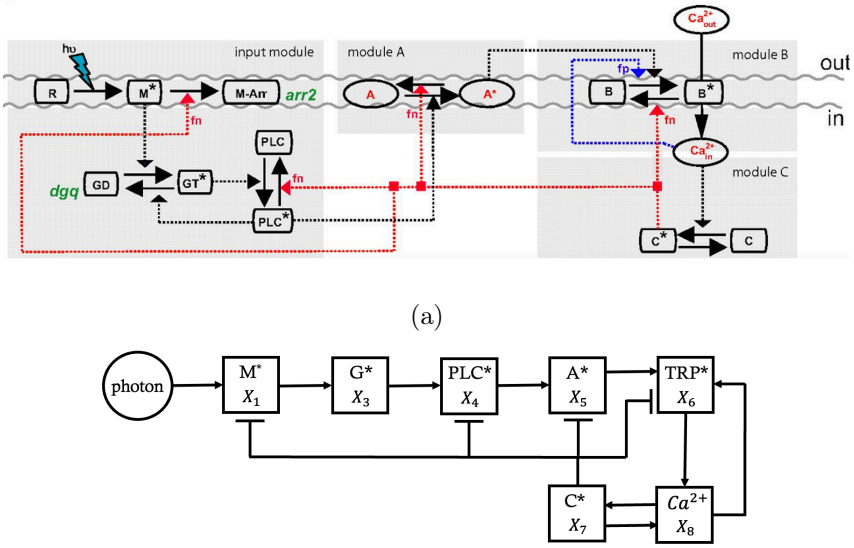

(a)

(b)

Figure 3. (a) The simplified molecular signaling cascade in a single microvillus [6]. (b) The diagram of the Full Model [4].

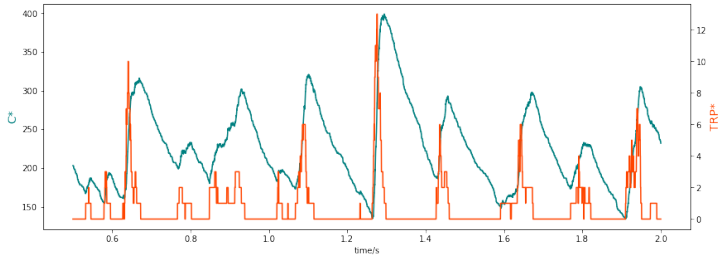

Figure 4. Given a constant input, the plot of the TRP channel (orange) and the C^* (green). From this we can see the quantum bump pattern and the refractory period induced by the C^* following each quantum bump

4.1. the original RPM: RPM0

All RPMs in this section are modified from the original RPM: RPM0, which is a 2 variables ODEs:

$$\frac{dx_1}{dt} = b_1 f(\lambda)(1 - x_1 - x_2) - b_2 x_1 - r x_1 x_2$$
$$\frac{dx_2}{dt} = b_2 x_1 - d_2 x_2$$
$$V = g(x_1)$$
$$f(\lambda) = \frac{b_0 \lambda}{b_0 \lambda + d_0}$$

where the g is a bijective linear map $g : [0, 1] \to [-82, -10]$, $f(\lambda)$ is the steady state of the kinetic equation:

$$\frac{dx_0}{dt} = b_0 \lambda (1 - x_0) - d_0 x_0$$

The RPM0 follows the similar construction of the model proposed by De Palo *et al.* [7], which characterizes the dynamical features of sensory adaptation in photoreceptors and olfactory sensory neurons in *Drosophila*. More specifically, the RPM0 aims to capture the transition between

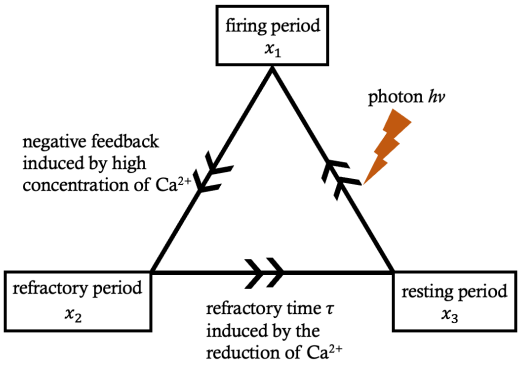

Figure 5. The triangle diagram of the transition between three states of a microvillus

microvilli states. Here x_1, x_2, $x_3 = (1 - x_1 - x_2)$ represents the ratio of microvilli in the firing period, the refractory period and the resting period respectively. It follows the conservation law since $\frac{d(x_1+x_2+x_3)}{dt} = 0$.

After receiving the photons, the microvilli in the resting period ($x_3 = 1 - x_1 - x_2$) will be activated via a transduction process. Partly due to its fast reaction speed and partly for simplicity, we replace the transduction reaction $\frac{dx_0}{dt} = b_0\lambda(1 - x_0) - d_0x_0$ with its equilibrium $f(\lambda)$. The activation will be followed by a refractory period. We also assume the microvilli in the refractory period will suppress the activation of microvilli via the Calcium negative feedback pathway.

RPM0, however, fails to capture the response curves of the Full Model with a wide range of luminance input. As is shown in **Figure 6**(a), although it can capture the bump response with high luminance, the response curves of RPM0 are different from most of the response curves of the Full Model. Thus, modification of RPM0 becomes necessary.

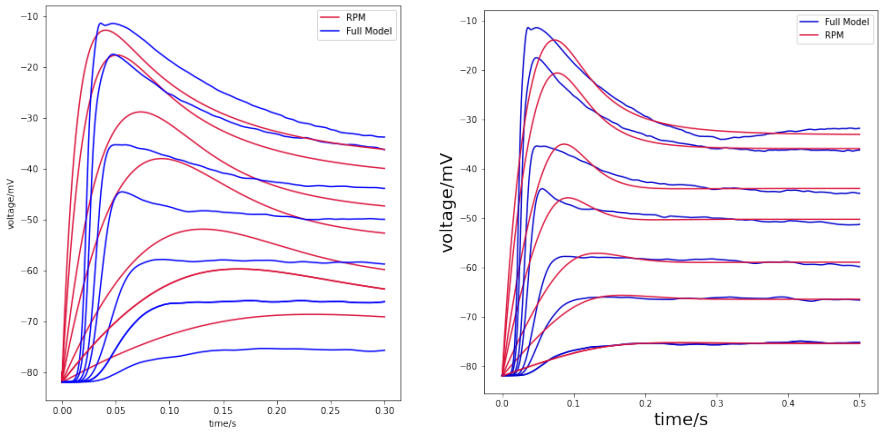

(a) (b)

Figure 6. (a) The comparison between the response curve of the RPM0 (red) and of the Full Model (blue) (b) The comparison between the response curve of the RPM1 (red, will be shown in 4.2) and of the Full Model (blue)

4.2. optimization method for RPMs with input dependent parameters

An essential observation is although RPM0 cannot capture the response curves of the Full Model with a wide range of luminance input, it can be optimized to fit the Full Model response curve with a fixed input, which could be written as an optimization problem:

Given a fixed luminance λ and an initial condition for RPM and the Full Model, try to find a set of parameters minimizing the loss function.

Suppose the loss function is the Mean Squared Error (MSE) and denote f as the solution of the Full model, $\hat{f}$ as the solution of a RPM.

$$\hat{\theta} = \arg\min \sum_{i=0}^{N} \frac{(\hat{f}(t_i|\theta) - f(t_i))^2}{N}$$

where $t_1, t_2, ..., t_N$ are the sampling time point.

However, such optimized $\hat{\theta}$ is determined for only one luminance λ. For different λ, the optimized parameters $\hat{\theta}$ are different. Thus, to make a RPM behave well in a world where luminance is always changing fast, we let the optimal parameters set θ be a function of λ, and use polynomials to make sure for every λ, the $\theta(\lambda)$ is always close to the best parameters set $\hat{\theta}(\lambda)$ (**Figure 7**).

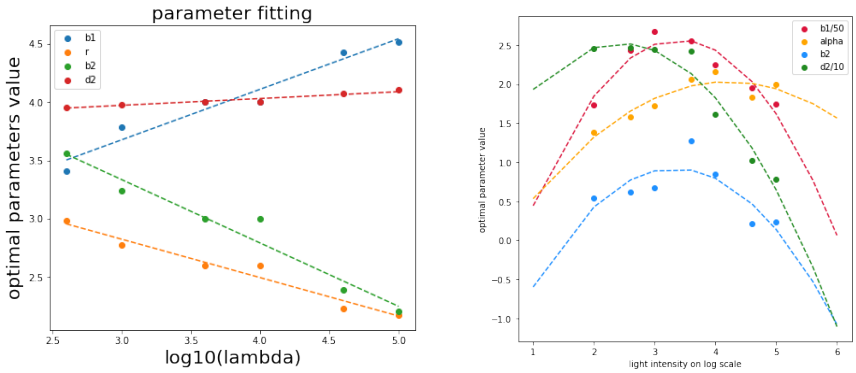

(a) (b)

Figure 7. (a) The optimal parameters as functions of λ in RPM4. (b) The optimal parameters as functions of λ in RPM1. Note that all the parameters should be positive.

The table below provides the detailed optimization strategy for RPMs:

Model	Parameters(λ)	deg of polynomial	loss function
RPM1	b1, α, b2, d2	2	weighted MSE
RPM2	b1, r, b2, d2	2	MSE
RPM3	b1, r2, b2, r3, b3, d3	3	MSE
RPM4	b1, r, b2, d2	1	two points error

where the two points error is defined by

$$w_1|V_{max} - \hat{V}_{max}| + w_2|V_{stable} - \hat{V}_{stable}| + w_3|t_{peak} - \hat{t}_{peak}|$$

i.e. the weighted sum of the absolute error of peak voltage, peak time, equilibrium voltage between a given RPM and the Full Model.
The weighted MSE is defined by

$$\sum_{i=0}^{N} w_i \frac{(\hat{f}(t_i|\theta) - f(t_i))^2}{N}, w_i = \frac{|f'(t)|}{\max(|f'(t)|)}$$

w_i is a weight based on the derivative. The faster the Full Model f changes, the more weight we give.

Thus, we can develop a series of RPM: RPM1-4, among which RPM1 has the best performance. The RPM1 is defined below with an exponential term, while other RPMs are defined in the

Appendix.

$$\frac{dx_1}{dt} = b_1(\lambda)f(\lambda)(1 - x_1 - x_2) - b_2(\lambda)x_1 - r(\lambda)(x_1x_2)^{\alpha(\lambda)}$$
$$\frac{dx_2}{dt} = b_2(\lambda)x_1 - d_2(\lambda)x_2$$
$$V = g(x_1)$$
$$f(\lambda) = \frac{1}{1 + e^{-y}}, \quad y = (\log_{10}(\lambda) - a_1) * a_2$$

4.3. performance test of RPMs

To test the performance of RPMs, we first test the its response of a given luminance input with background = 0. As is shown in **Figure 6**(b), RPM1 fits well with the response curves of the Full Model, except the delay of the peak voltage is slightly larger.

We further test RPM1's I/O relationship with a video input. From **Figure 8** (a) (also with a supplemental video), it is clear that the response of the RPM1 is similar to the response of the Full Model, with a low absolute error for each photoreceptor per frame. Note that the error is relatively large in the edge of the moving squid, which is where the luminance changes more drastically. This is because the time delay for the peak voltage when the luminance changes is larger in the RPM1 (**Figure 6**(b)), which is consistent with our observation of RPM1 as a single photoreceptor.

To quantitively define how much information is preserved, we use the Signal-to-Noise Ratio (SNR) to define the similarity between the RPM response and the Full Model response for each frame.

$$SNR = \frac{\sum_{i=1}^{N} x_i^2}{\sum_{i=1}^{N}(x_i - \hat{x}_i)^2}$$

where N is the number of photoreceptors in the retina (pixel number per frame), x_i is the output of the Full Model, $\hat{x}_i$ is the output of the RPM. Higher SNR represents higher similarity, i.e. better performance.

While RPM1 performs the best among all RPMs, both RPM1 and RPM3 have high SNR especially after the first 200ms (**Figure 8**(b)), indicating they both faithfully capture the behavior of the full model with little information loss. The low SNR in the first 200ms is due to the drastic change of background luminance from 0 to $\sim 1 \times 10^4$, which is what RPMs fail to capture. This could also be seen in **Figure 8**(c), which illustrates that the response of RPMs is always flatter than that of the Full Model when the luminance changes.

5. An Alternative RPM with PDE Description

In section 4, we construct RPMs with ODEs description. However, an unneglectable fact is that the luminance input dependent parameters fail to have a solid biological interpretation. To this end, here, we propose an novel approach for RPM from the integral-and-fire (IF) mechanism of microvilli with a Partial Differential Equation (PDE) description.

5.1. microvillus as an integral-and-fire device

In [6], Pumir *et al.* argue that the phototransduction cascade acts as an IF device. Although the Full Model is different from Pumir's quantitive model, we claim that the Full Model can also be viewed as an IF device.

As is shown in **Figure 9**(a), once the TRP channel activator A^* reaches a certain threshold (~ 30), it will activate the quantum bump instantly or with a time delay due to the stochastic nature of biochemical process. After that, the A^* will always decease to a low value. Otherwise, a quantum bump will not be triggered (yet there is still a small number of TRP channels opened) and A^* will go back to its 'resting state'.

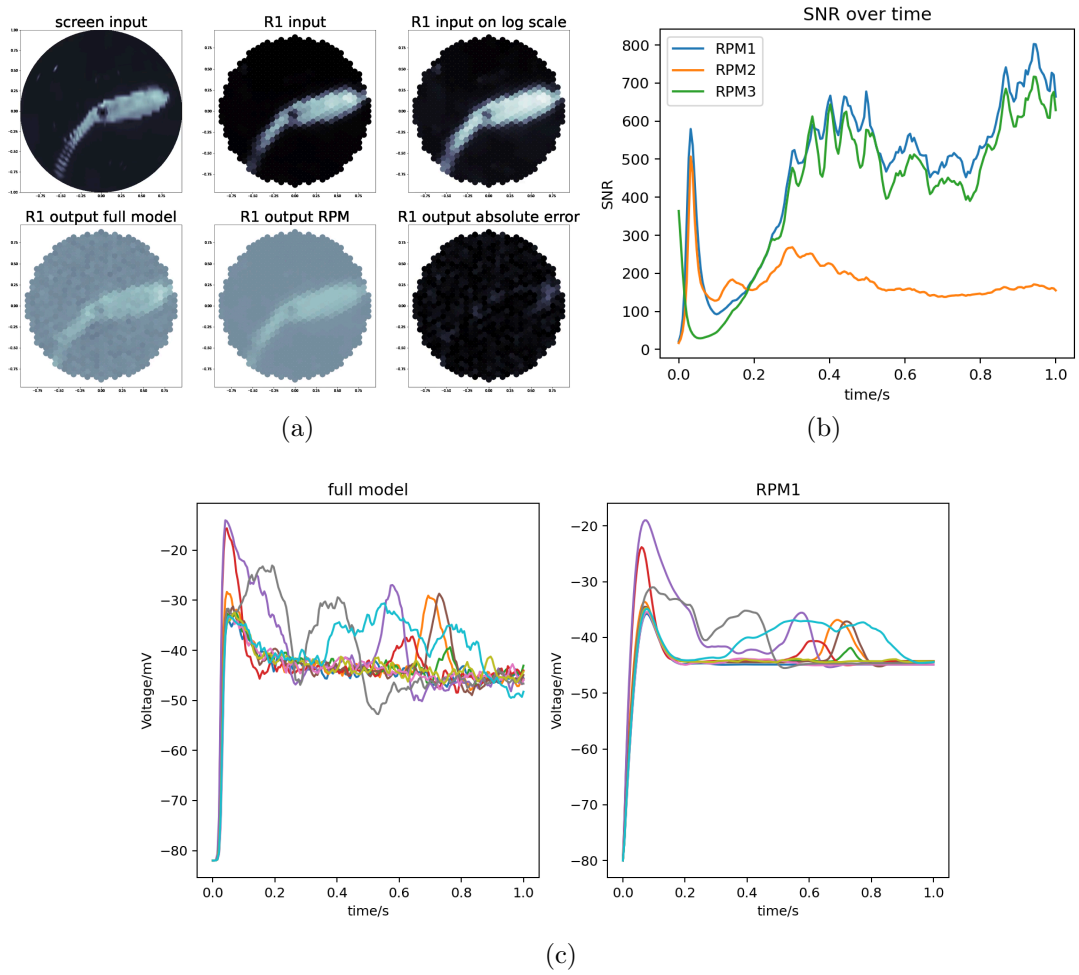

Figure 8. (a)The top row: the image projected on the screen, the actual input to the R1s in the retina, the input to R1s on log scale. The bottom row: the Full Model output, the RPM1 output, the absolute error between Full Model and RPM1 output. (b) The SNR versus time of RPM1-3. (c) The comparison between the Full Model and the RPM1 with randomly selected 10 photoreceptors.

Such a property is similar to the IF neuron, where once the voltage reaches a threshold, a spike will be triggered with the voltage reset to the resting potential. Otherwise, the voltage will decrease to the resting potential due to the leaky membrane.

Another observation is that the G protein G^* is almost $0/1$ over time (**Figure 9**(b)), suggesting that it could be viewed as a Poisson process with a changing Poisson rate η [8]. Thus, we can treat a microvillus as a IF neuron with a Poisson input of changing η.

5.2. a PDE description of microvilli population dynamic

With the IF device assumption, we can have a different approach to RPM. Suppose we have the firing rate m of the IF microvilli, then at each time step, we can get the number of microvilli in the firing state by Nm, where N is the number of microvilli. This is because the firing rate m is equal to the ratio of microvilli in the firing state x_1 when N is sufficiently large by the thermodynamic ensemble in statistical physics [9].

Since the quantum bumps are the major contribution to the opened TRP channels, we can always assume $\sum_N X_6 \approx Nm$. Thus, as is shown in **Figure 2**, we can compute the current I as well as the voltage V by the firing rate m.

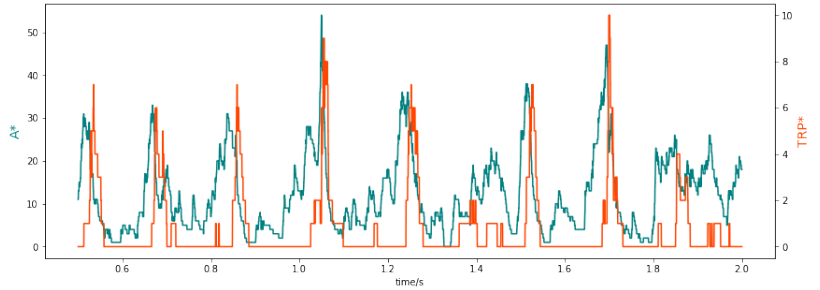

(a)

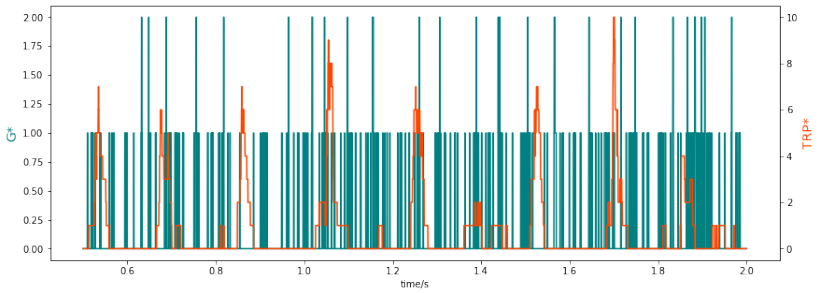

(b)

Figure 9. (a) Green: the A^* change over time. Orange: the TRP^* change over time. (b) Green: the G^* change over time. Orange: the TRP^* change over time.

Here, we give a novel method to calculate the mean firing rate m of the IF microvilli population with Poisson input based on the kinetics PDE [10] (the details of proof are omitted for briefness).

For simplicity, we assume the Poisson rate η is a constant and Poisson input will cause a instant A^* (or voltage in IF neurons) jump. The IF microvillus could de defined an IF neuron:

$$\frac{dv}{dt} = -g(v - v_L) + S^Y \delta(t - t_i)$$

where v represents the voltage in IF neurons and the TRP activator A^* in IF microvilli. S^Y, t_i represents the intensity and the time of Poisson input respectively.

We define the Probability Density Function (PDF) of v as $\rho(v, t)$. From the single IF microvillus equation, we can get the master equation:

$$\partial_t \rho(v,t) = g_L \partial_v [(v - v_L)\rho(v,t)] + \eta(\rho(v - S^Y, t) - \rho(v,t))$$

which can be rewritten as a Fokker-Planck equation:

$$\partial_t \rho(v,t) + g_L \partial_v J(\rho(v,t)) = 0$$

where

$$J(\rho(v,t)) = -(v - \mu)\rho(v,t) - \frac{\sigma^2}{2}\partial_v \rho(v,t)$$

$$\mu = v_L + \frac{\eta S^Y}{g_L}, \sigma^2 = \frac{\eta {S^Y}^2}{g_L}$$

The J represents the probability flow. μ, σ is the drift and diffusion term respectively.

The boundary condition here is $\rho(v_T, t) = \rho(\infty, t) = 0$, v_T is the threshold, by which, we can get the expression of the firing rate m using the flux at the threshold boundary.

$$m = g_L J(\rho(v_T, t)) = -g_L \frac{\sigma^2}{2}\partial_v \rho(v,t)$$

We can also get the steady state of firing rate m by normalizing the equilibrium solution:

$$\rho_{eq}(v,t) = \frac{2m}{g_L\sigma}\exp(\frac{(v-\mu)^2}{\sigma^2})\int_{\frac{v_R-\mu}{\sigma}}^{\frac{v_T-\mu}{\sigma}} e^{s^2}ds$$

However, such kinetics PDE is also expensive to numerically solve directly. Zhang *et al.* show that moment closure could turn this PDE into a set of augmented ODEs [11]. We define the moments as following:

$$M_j(t) = \int_{-\infty}^{v^T} v^j\rho(v,t)dv$$

by which we can transform the Fokker-Planck PDE into ODEs, which is easier to solve.

$$\frac{dM_j}{dt} = -mv^{Tj} - jg_L(M_j - \mu M_{j-1} - \frac{j-1}{2}\sigma^2 M_{j-2})$$

The solution of the Fokker-Planck equation ρ can be retrieved from the moments M_j. 4-6 moments are usually sufficient for an accurate approximation of the actual PDF $\rho(v,t)$, from which we can calculate the firing rate m, as well as the current I and voltage V.

6. Conclusion and Discussion

From previous sections, we have constructed the RPMs from the transition of microvilli states with an ODEs description (RPM with ODEs). Yet it captures response of the Full Model quite well with step function input and video input, we cannot neglect their lack of biological interpretation. Thus we come up with an alternative approach based on a kinetics PDE given the IF natural of microvilli (RPM with PDE). It directly comes from the physiological basis of microvilli with a statistic view, but still needs our further exploration. Both two types of RPM have their own strength and drawbacks, also implying the potential directions for improvement. We will discuss them separately.

For RPM with ODEs, **1)** it fails to capture the sharper and faster response in the Full Model when the luminance changes **2)** it has parameters dependent on the luminance input, which cannot be related to a solid biological explanation. **3)** it assumes the voltage V is a linear function of x_1 i.e. $V = g(x_1)$, which is not true due to the high non-linearity involved in the membrane model.

Thus, the potential directions to improve the RPM with ODEs are: **a)** Instead of letting $V = g(x_1)$, we aim to find a non-linear function linking the current and the x_1, i.e. $I = h(x_1)$. Then use the non-firing-membrane model to get the voltage V as the final output. Such construction follows the similar idea of the OSN-BSG model in the olfactory system of the *Drosophila* [12]. **b)** The interaction between x_1 and x_2 is rather simple, we can involve more non-linearity in the ODEs in interaction terms. RPM1 and RPM3 behaves well due to this reason, suggesting this method could be a right path. **c)** Reduce the number of parameters depending on the luminance as much as possible.

For RPM with PDE, **1)** the Fokker-Planck PDE is based on the constant Poisson rate η, which is not true since there is a negative feedback to G-protein G^* via C^*. **2)** how the luminance influences the Poisson rate of G^* remains unclear. **3)** The leaky term in the IF formula of A^* is for neurons, not for microvillus. **4)** whether the current can be calculated from the firing rate m is not tested.

Thus, the potential directions to improve the RPM with PDE are: **a)** Determine the Poisson rate η as a function of luminance λ and the firing rate m (since firing will trigger the negative feedback). **b)** Determine the leaky term of IF microvillus. **c)** Use the IF microvilli population with the result in a)b) to test whether the IF hypothesis holds, and if so, rewrite the Fokker-Planck equation.

Above all, as an I/O equivalence of the Full Model, both RPM with ODEs and RPM with PDE have shown their potential in dimension reduction for phototransduction simulation. While

keeping improving the RPM with ODEs, we would like to prioritize the development of RPM with PDE due to its solid physiological interpretation and non-trivial statistical insight. The IF property is not restricted to the photoreceptor, but widely spread in numerous biochemical cascades [13]. Thus, the RPM with PDE may have broader applications in quantitative biology.

We believe that the two types of RPM will both be able to faithfully capture the response of the Full Model with a solid biological interpretation. They are now being implemented into the large-scale whole circuit simulation of the visual system in the *Drosophila* by integration with amacrine cells layer and lamina via Neurokernel [14][15].

7. Appendix

7.1. RPM2, 4

Both RPM2 and RPM4 has the same formula. The only difference is the parameter functions $\theta(\lambda)$ are different.

$$\begin{aligned}
\frac{dx_1}{dt} &= b_1(\lambda)f(\lambda)(1-x_1-x_2) - b_2(\lambda)x_1 - r(\lambda)x_1x_2 \\
\frac{dx_2}{dt} &= b_2(\lambda)x_1 - d_2(\lambda)x_2 \\
V &= g(x_1) \\
f(\lambda) &= \frac{1}{1+e^{-y}}, \quad y = (\log_{10}(\lambda) - a_1) * a_2
\end{aligned}$$

7.2. RPM3

RPM3 is a 3 variables ODEs.

$$\begin{aligned}
\frac{dx_1}{dt} &= b_1(\lambda)f(\lambda)(1-x_1-x_2) - b_2x_1 - r_2(\lambda)x_1x_2 \\
\frac{dx_2}{dt} &= b_2(\lambda)x_1 - d_2x_2 - r_3(\lambda)x_2x_3 \\
\frac{dx_3}{dt} &= b_3(\lambda)x_2(1-x_3) - d_3(\lambda)x_3 \\
V &= g(x_1) \\
f(\lambda) &= \frac{1}{1+e^{-y}}, \quad y = (\log_{10}(\lambda) - a_1) * a_2
\end{aligned}$$

7.3. Recordings from the Full Model

Here are recordings from the Full Model. The orange lines are the opened TRP channels, while the green lines are molecular variable in the phototransduction cascade.

References

[1] Sterling, Peter, and Simon Laughlin. Principles of neural design. MIT press, 2015.

[2] Givon, Lev E., and Aurel A. Lazar. "Neurokernel: An open scalable software framework for emulation and validation of Drosophila brain models on multiple GPUs." Neurokernel Request for Comments, Neurokernel RFC 1 (2014).

[3] Kumar, Justin P. "Building an ommatidium one cell at a time." Developmental Dynamics 241, no. 1 (2012): 136-149.

[4] Lazar, Aurel A., Konstantinos Psychas, Nikul H. Ukani, and Yiyin Zhou. "A parallel processing model of the Drosophila retina. Neurokernel Request for Comments." Preprint at http://dx. doi. org/10.5281/zenodo 30036 (2015).

[5] Henderson, Stephen R., Helmut Reuss, and Roger C. Hardie. "Single photon responses in Drosophila photoreceptors and their regulation by Ca2+." The Journal of Physiology 524, no. 1 (2000): 179-194.

[6] Pumir, Alain, Jennifer Graves, Rama Ranganathan, and Boris I. Shraiman. "Systems analysis of the single photon response in invertebrate photoreceptors." Proceedings of the National Academy of Sciences 105, no. 30 (2008): 10354-10359.

[7] De Palo, Giovanna, Giuseppe Facchetti, Monica Mazzolini, Anna Menini, Vincent Torre, and Claudio Altafini. "Common dynamical features of sensory adaptation in photoreceptors and olfactory sensory neurons." Scientific reports 3, no. 1 (2013): 1-8.

[8] Othmer, Hans G., Steven R. Dunbar, and Wolfgang Alt. "Models of dispersal in biological systems." Journal of mathematical biology 26, no. 3 (1988): 263-298.

[9] Gibbs, Josiah Willard. Elementary principles in statistical mechanics: developed with especial reference to the rational foundations of thermodynamics. C. Scribner's sons, 1902.

[10] Cai, David, Louis Tao, Aaditya V. Rangan, and David W. McLaughlin. "Kinetic theory for neuronal network dynamics." Communications in Mathematical Sciences 4, no. 1 (2006): 97-127.

[11] Zhang, Jiwei, Yuxiu Shao, Aaditya V. Rangan, and Louis Tao. "A coarse-graining framework for spiking neuronal networks: from strongly-coupled conductance-based integrate-and-fire neurons to augmented systems of ODEs." Journal of computational neuroscience 46, no. 2 (2019): 211-232.

[12] Lazar, Aurel A., and Chung-Heng Yeh. "A molecular odorant transduction model and the complexity of spatio-temporal encoding in the Drosophila antenna." PLoS computational biology 16, no. 4 (2020): e1007751.

[13] Zhang, Qiang, Sudin Bhattacharya, Rory B. Conolly, Harvey J. Clewell III, Norbert E. Kaminski, and Melvin E. Andersen. "Molecular signaling network motifs provide a mechanistic basis for cellular threshold responses." Environmental health perspectives 122, no. 12 (2014): 1261-1270.

[14] Lazar, Aurel A., Nikul H. Ukani, and Yiyin Zhou. "Sparse identification of contrast gain control in the fruit fly photoreceptor and amacrine cell layer." The Journal of Mathematical Neuroscience 10, no. 1 (2020): 1-35.

[15] Lazar, Aurel A., Nikul H. Ukani, and Yiyin Zhou. "The cartridge: A canonical neural circuit abstraction of the lamina neuropil-construction and composition rules." In Neurokernel RFC 2. 2014.

.